



Influence of inhomogeneous cloud fields on optical properties retrieved from satellite observations

Jules R. Dim,¹ Tamio Takamura,¹ Itaru Okada,¹ Takashi Y. Nakajima,² and Hideaki Takenaka³

Received 6 August 2006; revised 28 February 2007; accepted 17 April 2007; published 3 July 2007.

[1] Analyses of solar radiation exchanges between the atmosphere and clouds are vital for the understanding of climate processes and cycles. Comparisons of satellite-to-satellite or satellite-to-ground-truth observations aiming at, elucidating the radiative behavior of atmospheric components (clouds, aerosols, gas, etc.), or validating data of a particular satellite are a common practice in global radiation investigations. In order to assess the quality of cloud optical properties derived from Geostationary Meteorological Satellite-5/ Stretched Visible Infrared Spin Scan Radiometer (GMS-5/SVISSR), the former procedure (satellite-to-satellite comparison) was used. Data derived from GMS-5/SVISSR satellite were compared with those from the polar-orbiting Terra-Moderate Resolution Imaging Spectroradiometer (Terra-MODIS) satellite. This comparison showed serious discrepancies between cloud optical depth (COD) data retrieved from the two satellites' observations. GMS-5/SVISSR-retrieved COD appeared mostly lower than that of Terra-MODIS. To understand the origin of such differences, an identification procedure of the major factors likely to affect these data is conducted. Some of these factors were the satellite viewing and solar conditions, the cloud thermodynamic phase differentiation and particle effective radius, and the cloud inhomogeneity. Then emphasis was put on the examination of the latter effect (i.e., the cloud inhomogeneity). The analysis procedure was as follows: First, data having close-viewing geometries between both satellites were selected and used to understand the effects of the remaining factors. Among these, the cloud thermodynamic phase appeared to play the major role as analyses showed that most of the COD differences between both satellites were confined within ice clouds while warm clouds had the least discrepancies. This would suggest that the choice of a water cloud particle radiative transfer model to analyze a 2-phase cloud radiation data, as used here, may produce large uncertainties in ice COD retrievals from at least one of the satellites. To avoid the cloud phase problem, a more restrictive data set comprising only water clouds (besides close-viewing geometries between both satellites) was selected, and the impact of the degree of cloud inhomogeneity on the COD retrievals was evaluated. The study reveals that the 3-D radiative effects deriving from the external cloud inhomogeneity, i.e., cloud asymmetry and structured sides, were the most influencing properties here. The GMS-5/SVISSR interpretation of inhomogeneous cloud optical properties showed larger uncertainties than that of Terra-MODIS. Furthermore, COD values of GMS-5/SVISSR were systematically lower than those of Terra-MODIS for the pixels at shadow sides of the cloud, while at illuminated sides they often showed higher values. For gentle or near-plane-parallel cloud surfaces, fewer discrepancies were noticed (the best agreement between both satellites' retrievals). At steep slopes of the shadow and illuminated cloud sides, GMS-5/SVISSR average COD data were respectively under- and overestimated

¹Center for Environmental Remote Sensing, Chiba University, Chiba, Japan.

²Department of Network and Computer Engineering, School of Engineering II, Tokai University, Tokyo, Japan.

³Graduate School of Science and Technology, Chiba University, Chiba, Japan.

compared to those of Terra-MODIS. COD differences between the two satellites could be sometimes higher than 30% for slopes steeper than 0.5 K/km.

Citation: Dim, J. R., T. Takamura, I. Okada, T. Y. Nakajima, and H. Takenaka (2007), Influence of inhomogeneous cloud fields on optical properties retrieved from satellite observations, *J. Geophys. Res.*, 112, D13202, doi:10.1029/2006JD007891.

1. Introduction

[2] Clouds interfere with the transfer of radiation in the atmosphere in two ways: Firstly, they reflect a certain proportion of solar radiation back to space, so reducing the total energy available to the system; secondly, they act as blankets to thermal radiation from the Earth's surface in a similar way to greenhouse gases [Houghton, 2002]. The study of cloud properties is therefore of prime importance in the understanding of heat exchange processes of the Earth. To view these clouds and other atmospheric components as a whole disk rather than in subsections, geostationary satellites are the most suitable instruments. The other main advantages these satellites present are they observe the Earth from a stationed position (about 36,000 km) and monitor changes of atmospheric phenomena at short time intervals (data are recorded every hour or half hour). This high temporal resolution makes them very appropriate tools for global analyses. However, because of the relatively low spatial resolution and postlaunch progressive degradation of the sensitivity of the sensors onboard these satellites, the data they observe need to be calibrated and validated. In general the calibration and validation processes are conducted either by comparing the data obtained from these instruments with ground-truth data or with a higher spatial resolution satellite (generally polar orbiting). Various works have been conducted with such comparisons either for calibration and validation purposes or with the aim of evaluating the impact of atmospheric radiative properties on the Earth. Among these, one of the most prominent is that of the International Satellite Cloud Climatology Project (ISCCP), which provides systematic calibration schemes of geostationary satellites on the basis of National Oceanic and Atmospheric Administration (NOAA) polar orbiting satellites [Rossow *et al.*, 1992; Desormeaux *et al.*, 1993; Brest *et al.*, 1997]. Other works include Le Marshall *et al.* [1999], who use collocated nadir observations to calibrate the radiances from the Visible Infrared Spin Scan Radiometer (VISSR) instrument on Geostationary Meteorological Satellite-5 (GMS-5) by comparing this satellite's data with those of the Advanced Very High Resolution Radiometer (AVHRR) instrument on NOAA. Minnis *et al.* [2002] propose a calibration method of operational and research meteorological satellite imagers' visible channels, based on correlating the Visible Infrared Scanner (VIRS) on Tropical Rainfall Measuring Mission (TRMM) and the second Along-track Scanning Radiometer (ATSR-2) with the matched data from Geostationary Operational Environmental Satellite-8 (GOES-8), GMS-5, Terra-MODIS, then Visible and Infrared Scanner (VIRS) with Clouds and the Earth's Radiant Energy System (CERES). Kriebel *et al.* [2003] make comparisons of cloud data retrieved from surface observations, in order to improve and validate the AVHRR Processing scheme Over Clouds, Land and Ocean (APOLLO). Picon and Desbois [1995] summarize and interpret the main applications of the water vapor Meteosat

channel in comparison with GOES and GMS. Casanova *et al.* [2005] use visible and infrared channels of the Meteosat satellite alongside data provided by the Advanced/Tiros-N Operational Vertical Sounder (A/TOVS) probe onboard NOAA polar satellites to derive a cloud classification method for civil aviation applications. Nowicki *et al.* [2003] compare cloud microphysical properties derived from AVHRR data to those of MODIS, VIRS, and GMS over the tropical western Pacific in order to understand differences between the resulting products and similar quantities derived from other satellites. Yi *et al.* [2001] propose a multiangle satellite data set using GOES-East, GOES-West, GMS-5, MODIS, and NOAA. Chang *et al.* [2000] use coincident and collocated Earth Radiation Budget Experiment (ERBE) and AVHRR observations to examine the dependence of both shortwave top-of-atmosphere reflectance and albedo on cloud optical properties. Most of these studies highlight the fact that the quality of satellite cloud data observations does not only depend on satellite sensors' electronic performance (signal stability) but also on the atmospheric conditions, the solar and viewing geometries, the intrinsic characteristics of the clouds (degree of cloud homogeneity), and the capacity of the radiative transfer models to properly interpret field direct satellite observations. Because of these hindrances, the characterization of cloud reflected radiance from satellite data might not always be straightforward. The common interpretation of cloud optical properties is based on one-dimensional (1-D), or homogeneous and plane-parallel radiative transfer models neglecting any net horizontal radiation flux between pixels [Marshak *et al.*, 1998]. 1-D retrievals can estimate clouds to be too thin or thick, too smooth or rough, artificially anisotropic, and asymmetric [Varnai and Marshak, 2002]. Satellite cloud properties may therefore be biased because of various factors like 3-D radiative effects resulting from cloud inhomogeneities. For example, cloud optical depth retrieved using radiative transfer theory without prior knowledge of a structured cloud top will systematically be overestimated for sunlit sides and underestimated for cloud sides in the shade [van Hees and Lelieveld, 2000]. Various attempts to obtain simple approximations in the identification of the incident and reflected photon trajectory on inhomogeneous media have been made during recent years. Many of these studies use radiative transfer models based on the Monte Carlo ray tracing approach to explain the complex influence of cloud heterogeneities on the reflected radiation and show that reflection from structured cloud surfaces may be significantly different from that of flat-top clouds [e.g., Loeb *et al.*, 1997; Varnai and Davies, 1999; Iwabuchi and Hayasaka, 2002]. The degree of accuracy of these approximations has a significant impact on the global-scale radiation computation. Because of the nonlinear dependence of cloud albedo on cloud optical depth, errors in cloud optical depth lead to

large errors in cloud albedo, and therefore energy budget calculations [Loeb and Coakley, 1998].

[3] Within the framework of the Asian Atmospheric Particulate Environment Change Studies–Experiment 2 (APEX-E2) project, intensive field campaigns including ground-based measurements, ferry boat measurements, and aircraft measurements, as well as satellite remote sensing and model simulation of radiation, aerosols, and cloud characteristics [Nakajima *et al.*, 2003], were conducted during the month of April 2001. To extend the findings of these experiments to at least the regional scale or fill the gaps between the sparse ground-based measurement stations, the use of a high temporal resolution satellite coverage such as that provided by GMS-5 was suggested. As most geostationary satellites, GMS-5 has a lower spatial resolution than many low-altitude satellites such as the polar orbiters. Because of this resolution difference, the latter can serve as a validation tool for the geostationary satellite. This is the approach, which motivated the present study. GMS-5/SVISSR-retrieved cloud microphysical and optical data are compared with that of the polar-orbiting Terra-MODIS. The consistency of cloud properties retrieved from GMS-5/SVISSR satellite can by this way be evaluated as well as the performance of its observations at various cloud conditions and geometries. Qualitative and quantitative estimates of the differences between cloud properties retrieved from both satellites (GMS-5/SVISSR and Terra-MODIS) are presented. Daily cloud radiation data recorded by both satellites during the APEX-E2 field campaign period (April 2001) are used for these analyses. The scenes studied cover an area off the East China Sea (25–35°N and 125–135°E). Results of this comparison show that GMS-5/SVISSR cloud optical depth (COD) values are mostly lower than those of Terra-MODIS. To understand the origin of such differences and identify the major factors likely to have affected these data, a graduated processing scheme of data selection is conducted. This examination reveals that the COD retrieved had some dependence on the cloud thermodynamic phase. In fact, the major COD differences between both satellites were mostly confined in the ice clouds while the warm clouds showed few or minimum discrepancies. This would suggest that the choice of a water cloud particle radiative transfer model to analyze a 2-phase cloud radiation data (as adopted in this study) may produce large uncertainties in ice COD retrievals from at least one of the satellites. A restrictive data set including only water clouds is then reanalyzed to check the impact of other factors with a particular emphasis put on the degree of cloud inhomogeneity. The most influential inhomogeneity elements here are the 3-D radiative effects (asymmetry and cloud top structures) due to the external cloud inhomogeneity. This study shows that shadow cloud sides behave differently from the sunlit sides. The 3-D radiative effects appear to cause more uncertainties in the COD retrieved from GMS-5/SVISSR than those from Terra-MODIS. In the examination of the asymmetry component of these radiative effects, it was noticed that the GMS-5/SVISSR COD values of the pixels at shadow sides of the cloud are, on average, systematically lower than those of MODIS, while at illuminated sides they increased and are often higher than the latter. The other component of the radiative effects, the cloud top structure analysis, shows that near-plane-parallel surface clouds have

few discrepancies and therefore the best agreement between both satellites' retrievals.

[4] The outline of this paper stands as follows. Subsequent to this introduction, observation conditions of the retrieved data and satellites characteristics are presented in section 2. In section 3, factors likely to affect satellite cloud observations and the optical depth retrievals are discussed. It results from this discussion that the differences in the retrieved COD strongly depend on the cloud thermodynamic phase and therefore the choice of the cloud phase radiative transfer model. Hereafter, only water clouds are selected for the remaining analyses; and, in order to avoid ice contamination, a sufficiently high temperature threshold for water cloud discrimination is imposed, i.e., above Infrared brightness temperature difference (IR BT) of 265 K on close-viewing geometry data. On the basis of this reduced data set, possible cloud inhomogeneity effects on COD retrievals from both satellites are analyzed and presented in section 4 of this paper. Internal inhomogeneity due to the cloud extinction coefficient and external inhomogeneity due to cloud radiative effects are evaluated. Finally, section 5 summarizes the main results obtained in this study.

2. Satellite Characteristics and Observation Conditions

[5] In order to evaluate cloud products from GMS-5/SVISSR, comparisons are made with retrievals from Terra-MODIS. The cloud properties analyzed are based on scenes having a spatial resolution of $0.05 \times 0.05^\circ$ ($5 \times 5 \text{ km}^2$) and a discretized grid of 200×200 cells. GMS-5/SVISSR daily scenes most temporally coincident with those of Terra-MODIS are selected for the study. The time difference between the scenes varies from 3 to 28 min. Visible ($0.55\text{--}0.90 \mu\text{m}$ for GMS-5/SVISSR and $0.841\text{--}0.876 \mu\text{m}$ for Terra-MODIS), infrared ($10.5\text{--}11.5 \mu\text{m}$ and $11.5\text{--}12.5 \mu\text{m}$ for GMS-5/SVISSR and $10.78\text{--}11.28 \mu\text{m}$ and $11.77\text{--}12.27 \mu\text{m}$ for Terra-MODIS), and near-infrared ($1.628\text{--}1.652 \mu\text{m}$ and $3.66\text{--}3.84 \mu\text{m}$ for Terra-MODIS) channels are used for the retrieval of cloud optical and microphysical properties (optical depth, cloud top height, particle size effective radius, and liquid water path). The GMS-5 satellite is located at nominal geodetic coordinates of 0° latitude and 140°E longitude, and its sensor SVISSR scans west to east. The Terra satellite sun-synchronous, and its sensor MODIS, scans at an angle that depends on latitude and generally in a northwest–southeast direction. The initial pixel's resolutions at nadir for GMS-5/SVISSR and Terra-MODIS visible channels (VIS) are respectively 1.25 and 1 km. For the Infrared channels (IR), they are, respectively, 5 and 1 km. In order to match the GMS-5/SVISSR IR channel spatial resolution, the initial pixel resolution of this satellite's visible channel and that of all Terra-MODIS channels used is degraded to a size of 25 km^2 , by simple averaging. GMS-5/SVISSR IR radiometric resolution is 0.35 K at 300 K and 1.00 K at 220 K [MSC, 1997]. Terra-MODIS absolute temperature accuracy is 0.2 K over oceans and 1 K over land. Temperature differences at Terra-MODIS 11μ channel as small as 0.01 K are reported in the images, and the noise equivalent temperature difference is about 0.05 K [Varnai and Marshak, 2001].

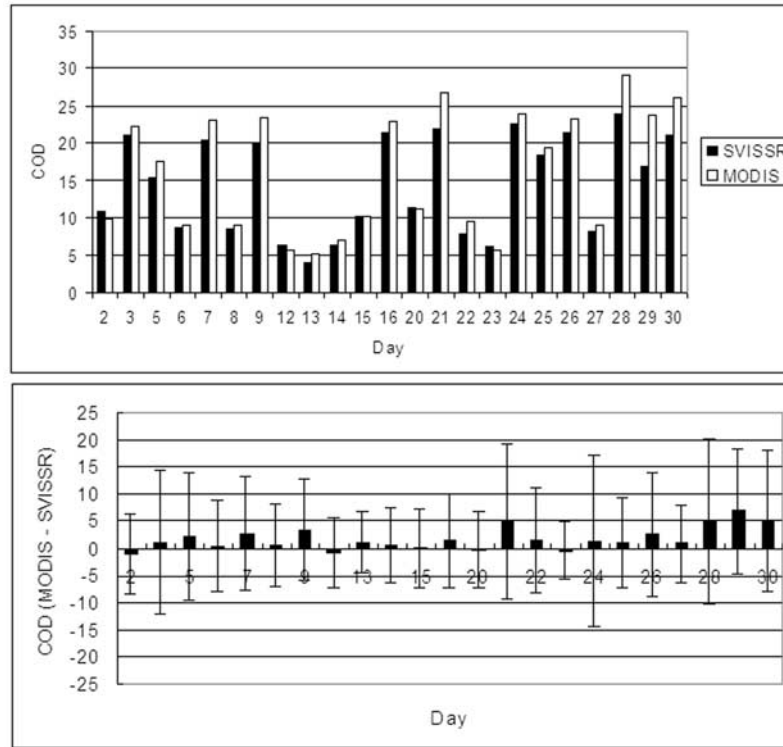


Figure 1. (top) Comparison of Geostationary Meteorological Satellite-5/Stretched Visible Infrared Spin Scan Radiometer (GMS-5/SVISSR) and Terra-Moderate Resolution Imaging Spectroradiometer (Terra-MODIS) cloud optical depth (COD) data on cloudy days of the month of April 2001. (bottom) Daily mean differences. The vertical bars represent the COD root-mean-square difference (RMSD).

[6] The algorithms used for both satellites' cloud optical and microphysical data retrievals are water cloud phase algorithms. They are based on the radiative transfer theory for plane-parallel layers with an underlying Lambert surface and use the solar reflectance method. This method takes advantage of the properties of water-absorbing near-infrared wavelengths to simultaneously retrieve the cloud optical depth and effective particle radius. Cloud top temperature and height are also derived from these computations. All particles' retrievals are assumed spherical and water phase. For cloudy and clear-sky pixels' discrimination, specific thresholds, using the ISCCP cloud classification [Rossow and Garder, 1993] and the split window technique, are applied. Cloud optical depth and effective particle radius are determined from radiances by using an inverse method of lookup tables. These lookup tables are generated at different viewing geometries by using the RSTAR-5b code [Nakajima and Tanaka, 1988]. The optical depth retrieval procedure from both satellites has a structure similar to that provided by Nakajima and Nakajima [1995] and Kawamoto *et al.* [2001]. Because of saturation problems on the reflected solar radiation, the cloud optical thickness retrieval accuracy is poor above 70. The low sensitivity of the reflectance to very high or extremely low optical depth values makes COD retrievals to be mostly reliable between 1 and 70. As no near-infrared channel around 3.7–3.9 μm band is available on GMS-5/SVISSR, cloud particle effective radius cannot be retrieved, it is therefore assumed as 10 μm . For Terra-MODIS the particle effective radius retrievals yield values ranging from 2 to 30 μm for the cloud scenes

analyzed in this study. Terra-MODIS products used in the cloud retrievals are calibrated, geolocated radiance data with a 12-bit quantization. The GMS-5/SVISSR digital counts (6 bit for VIS and 8 bit for IR) products are converted to reflectance by using the calibration coefficients suggested by MSC [1997]. The bidirectional reflection function for each pixel is calculated from radiances following Loeb and Coakley [1998]:

$$R(\tau_p; \mu, \mu_0, \phi) = \frac{\pi I(\tau_p; \mu, \mu_0, \phi)}{\mu_0 F} \times 100\% \quad (1)$$

with I = pixel radiance ($\text{Wm}^{-2} \text{sr}^{-1} \mu\text{m}^{-1}$), F = solar irradiance ($\text{Wm}^{-2} \mu\text{m}^{-1}$), τ_p = cloud optical depth, μ = cosine of observer zenith angle, μ_0 = cosine of solar zenith angle, and ϕ = azimuth angle relative to the solar plane ($\phi = 0$ corresponds to forward scattering).

[7] The distribution of the Earth's global radiation is primarily governed by the cloud amount. To attain high accuracy in the evaluation of the Earth radiation budget, uncertainties due to COD retrievals must be reduced [Cahalan *et al.*, 1994]. The problem in remote sensing data is generally the degree of reliability of products obtained from a particular satellite. A way to check this is a comparison with other satellites' data. The present work examines the conditions under which COD retrieved data from GMS-5/SVISSR and Terra-MODIS agree or differ from each other. Initial examination of the daily cloud scenes selected shows that the COD obtained may remarkably differ from one satellite to the other. Figure 1 presents

the COD daily mean, differences, and root-mean-square (RMSD) difference for the cloudy days of the month of April 2001. GMS-5/SVISSR COD values appear regularly lower than those of Terra-MODIS. These differences increase with the cloud thickness. On days with thinner clouds, COD discrepancies are less remarkable. The RMSD shows the degree of data scattering.

[8] To quantify the discrepancies between retrievals from these satellites, the following quantities are used: the simple COD difference, i.e., Terra-MODIS minus GMS-5/SVISSR, and the relative frequency (RF) defined as the ratio or frequency (in %) of Terra-MODIS pixels with COD values higher than that of GMS-5/SVISSR.

$$RF(\%) = \frac{\text{Number}(\text{MODIS}_{\text{COD}} > \text{SVISSR}_{\text{COD}})}{N} \times 100 \quad (2)$$

where N is the total number of data (or pixels) considered.

[9] Satellite observations as well as optical and micro-physical data retrievals are affected by various factors. Here is an account of the most important of them, presented and discussed according to the following order: (1) satellite viewing and solar geometries, (2) cloud thermodynamic phase differentiation and particle effective radius, (3) sensors' resolution, spectral channel bandwidth, and data quantization, (4) calibration and geolocation problems, and (5) cloud inhomogeneity 3-D radiative effects. Section 3 will try to weight the impact of these factors on COD retrievals and differences between both satellites.

3. Satellite Observations and COD Retrievals Influencing Factors

[10] In this section, the major factors influencing satellite observations and retrievals, likely to be at the origin of the COD discrepancies noticed between GMS-5/SVISSR and Terra-MODIS, are progressively discussed (in the order introduced at the end of section 2). Additionally, the data clearly affected till the last-but-one factor will be progressively discarded. Then the remaining data will be evaluated to understand the impact of cloud inhomogeneity.

3.1. Satellite Viewing and Solar Geometries

[11] Because Terra-MODIS observations widely vary in many of the scenes of this study (viewing angles range from 0 to 70°) and show a relative azimuth angle in the near forward or near backward scattering view or both (here 0° corresponds to the forward scattering view, while 180° is the backward scattering view), they are likely to be biased mainly at large viewing angles. GMS-5/SVISSR scenes have constant satellite zenith angles, always confined in a narrow range of less than 15° (30–45°) and a relative azimuth angle in the near backward scattering viewing direction, i.e., 155–180°. As suggested by *Loeb and Coakley* [1998], when 1-D reflectances are directly compared with observations at different view angles, relative differences are generally small in the backscattering direction for solar zenith angles $\leq 60^\circ$ and show no systematic view angle dependence, and it would be recommendable that direct application of the plane-parallel model approximation be restricted to moderate-high sun elevations and to view angles in the backscattering direction. For better

comparisons of COD retrievals, only Terra-MODIS data closely matching the viewing conditions of GMS-5/SVISSR will be selected for the remaining analyses, i.e., data in the near backward viewing direction and satellite viewing angles comprised between 30 and 45°. For the scenes examined the solar zenith angle is mostly below 36°.

3.2. Cloud Thermodynamic Phase and Particle Effective Radius

3.2.1. Cloud Thermodynamic Phase

[12] In this section, we examine the influence of the choice of a water cloud radiative transfer code on the COD retrieved from a set of data containing both ice and water cloud phases. Only closely matching viewing geometry data as selected from section 3.1 are analyzed here. Retrievals' processing algorithms of both satellites are water phase type with almost similar features except the fact that retrieval of the cloud effective radius is only possible with Terra-MODIS (at the near IR channel: 1.628–1.652 μm) while it is assumed 10 μm for GMS-5/SVISSR. Because water and ice cloud particles differ by their shape, size, and orientation, the energy they transmit and reflect would be different as well. According to their altitude, clouds are designated as –low (or –warm) and –high (or –cold). Parameters such as the cloud horizontal extension, the optical depth, the cloud morphology, etc., combined with atmospheric pressure and cloud brightness temperature, are commonly used for cloud classification. In order to examine how the cloud vertical development could affect the proper retrieval of their optical depth, a classification method based on the split window technique [*Inoue*, 1987], i.e., the brightness temperature difference (BT) between 11 μm and 12 μm channels, is applied on the data of this study. This classification shows that most of the COD differences between GMS-5/SVISSR and Terra-MODIS occur in the cumulonimbus (Cb) and cirrus (Ci) clouds. The best agreement is obtained with cumulus (Cu) clouds. Cb clouds are cold clouds (IR BT < 250 K) while Cu are warm clouds (IR BT > 250 K). For days with enough Ci clouds, the coldest among them show the largest optical depth discrepancy. Warmer Ci clouds have fewer discrepancies. Warm clouds are per definition water phase clouds, while cold clouds are ice phase. The comparison of COD between GMS-5/SVISSR and Terra-MODIS shows, therefore, that the COD differences (MODIS – SVISSR) tend to be larger in high and consequently cold clouds than in low and warm clouds. Figure 2 presents these differences for all the daily scenes having enough cold and warm cloud data then among these, the scenes with forward viewing geometry and closely matching satellite zenith angles. It can be seen that large COD differences in ice clouds occur as well in opposite viewing directions, i.e., near backward for GMS-5/SVISSR and near forward for Terra-MODIS (2, 5, 7, 9, 14, 16, 25, 28, and 30 April) as in similar ones, i.e., backward viewing for the two satellites (3, 24, 26, and 29 April). The RF is always higher (more than 50% of the total data) in ice cloud areas. A much more reasonable percentage ($\sim 50\%$) is obtained with water clouds. Average COD differences (MODIS – SVISSR) in ice clouds can be as high as 16 (e.g., 30 April, where MODIS optical depth is around 26), while in water clouds the differences are confined within COD values of less than 4. This classification of satellite

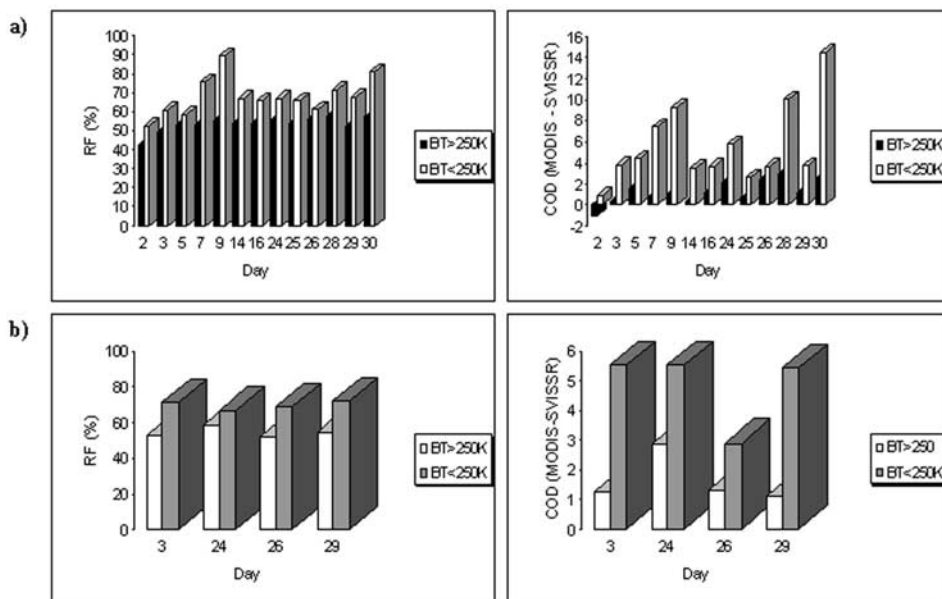


Figure 2. (a) Cloud thermodynamic phase difference. Ice clouds are designated by brightness temperature difference (BT) < 250 K, while water clouds have BT > 250 K. All days with enough cold and warm cloud data are represented. (b) Same as Figure 2a, but for daily scenes with forward viewing geometry and closely matching satellite zenith angles. The ordinate axes are relative frequency (RF) and COD (MODIS – SVISSR), i.e., cloud optical depth difference between MODIS and SVISSR (right).

data according to the cloud BT confirms that large COD discrepancies mostly occur in high clouds (ice phase). Low clouds (water phase) show fewer discrepancies.

[13] The large differences (MODIS – SVISSR) noticed in the ice clouds may suggest that ice phase interpretation with a water droplet algorithm could be problematic. The choice of a water cloud particle radiative transfer model to analyze a 2-phase cloud radiation data may produce large uncertainties in ice cloud optical depth retrievals of at least one of the satellites. *Minnis et al.* [1993], in a comparison of a geostationary satellite (GOES) cloud optical depth retrievals of cirrus clouds with those of a polar-orbiting satellite (AVHRR), use four radiative transfer models (one based on water droplets and three based on ice crystals) and show that the largest differences between the two satellites occur with the water droplet model. In this model, the AVHRR optical depths are larger (67%) than the GOES values over the entire range of optical depths. The interpretation of cirrus reflectance with water droplet models can lead therefore to biased results. This could be the case of our study as well as many others dealing with ice clouds. In our case, the use of a water droplet phase model to interpret radiances from ice clouds leads systematically to higher values of optical depths by the polar-orbiting Terra-MODIS compared to the geostationary GMS-5/SVISSR. Other reasons explaining this situation could be the cloud particle effective radius distribution. The distribution histogram of the effective radius of these cloud particles presented by Figure 3 shows that the frequency of these data is predominantly around $10 \mu\text{m}$ (value used for GMS-5/SVISSR COD retrievals) for water clouds and much higher values for ice clouds. This distribution difference could be at the origin of the discrepancies between ice and water clouds COD. The main difference between the models used for the

COD retrievals is the assumption of an effective radius for GMS-5/SVISSR ($10 \mu\text{m}$). This fixed value appears to work well with water clouds but behaves poorly with ice clouds. Because of the uncertainties of the water cloud models used to retrieve ice clouds COD, only water clouds (IR brightness >250 K) will be used for the remainder of our analyses. Furthermore, to avoid possible contamination of the data sets by some remnant ice clouds (so as only water clouds pixels are selected), the brightness temperature threshold will be increased to 265 K. Therefore in the remainder of this work, i.e., section 3.2.2 to section 4, only data with $\text{BT} \geq 265 \text{ K}$ will be used. Besides, and in order to reduce some of the effects of the scanning time differences and possible satellites' misalignment problems, a further condition (2 K maximum IR brightness temperature difference between both satellites) is introduced.

3.2.2. Cloud Particle Effective Radius

[14] As recommended by the ISCCP, when the retrieval of cloud particle effective radius is not possible, a $10 \mu\text{m}$ radius is assumed [Rossow, 1989]. This case applies to GMS-5/SVISSR COD retrievals, as no water channel sensor is available on this satellite. The cloud particle effective radius as retrieved from Terra-MODIS shows values ranging between 2 and $30 \mu\text{m}$. This distribution shows however a widely dominant mode at $10 \mu\text{m}$ and is generally correlated with the cloud temperature distribution. Low or water clouds show mostly smaller cloud particle effective radius values while high or ice clouds have generally high values. Retrieval tests (not shown) made with the GMS-5/SVISSR retrieval algorithm, assuming maximum ($30 \mu\text{m}$) and minimum ($2 \mu\text{m}$) effective radii, did not yield substantial COD differences (less than 1.8%) compared with those obtained by assuming a $10 \mu\text{m}$ cloud particle effective radius. *Loeb and Coakley* [1998], studying the variation

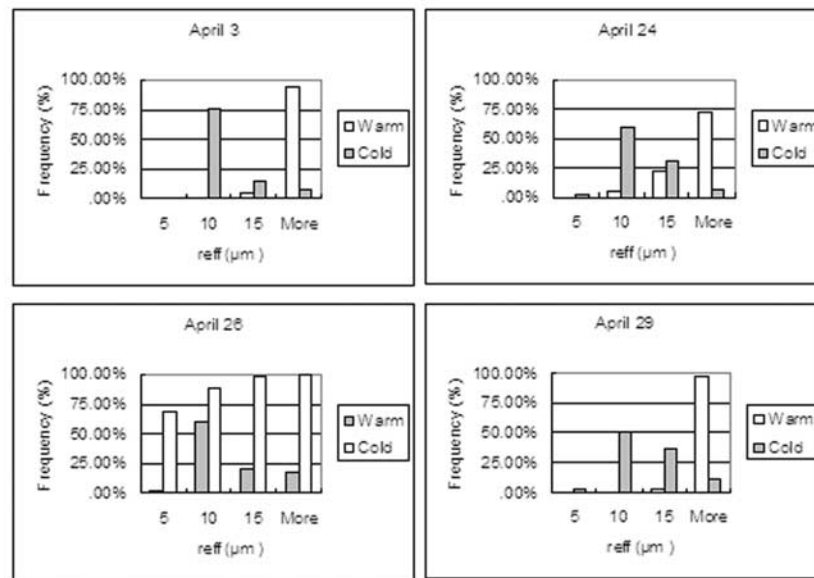


Figure 3. Cloud particle effective radius (“reff”) distribution for warm (“Warm”) and cold (“Cold”) clouds of similar days as in Figure 2a.

of reflectance with the viewing geometry for a wide range of atmospheric models (particle effective radii of 6, 10, and 20 μm), show that relative differences in 1-D reflectance due to drastic changes in cloud microphysics are less than 2%. The comparison, at similar cloud heights (i.e., clouds having temperature differences of less than 1 K) of the variability of Terra-MODIS COD and droplet effective radius, shows a very weak or no correlation at all between the two parameters (Figure 4). This suggests that the remaining differences between water clouds COD of the two satellites may not be primarily related to the variability of the effective radius. Differences will likely occur at individual pixels (this could be one of the factors at the origin of the more or less increased dispersion around the mean COD differences between the two satellites). Because the effective radius distribution of the scenes of this study is centered on 10 μm , there will be an overall effect of compensation for the COD differences in water clouds when means are computed.

3.3. Sensors’ Resolution, Spectral Channel Bandwidth, and Data Quantization

3.3.1. Sensors’ Resolution

[15] Terra-MODIS spatial resolution at nadir (1 km) is 25% higher than that of GMS-5/SVISSR (1.25 km). Generally, the higher the satellite resolution, the better it would allow for the detection of thinner clouds. To avoid this problem, clouds with $\text{COD} < 1$ were preliminarily excluded from our analyses. The visible spectral channel bandwidth is broader in GMS-5/SVISSR (0.55–0.90 μm) than in Terra-MODIS (0.862–0.877 μm). For degraded pixel sizes, or low spatial resolution sensors, frequent contamination of dark clear-sky, partially overcast, and broken cloud pixels may occur; and these are likely to reduce the COD. Oreopoulos and Davies [1998] suggest that the neglect of the subpixel cloud fraction introduces underestimates of cloud optical depth, which grow with pixel size, since larger pixels are more often partially cloudy. They explain as well

that some low values of cloud optical depth retrievals can be due to the reduction in the average reflected radiance from the clear portion of large pixels (cloud fraction effect), but it is only when high-resolution radiometric data become routinely available, that it will be possible to examine more effectively resolution effects on plane-parallel homogenous albedo bias. Loeb and Coakley [1998] provide a quantitative estimate of the relative uncertainty in reflectance, due to changes in pixel resolution with view angle, and show that reflectances from degraded resolution pixels tend to be lower than those obtained at full resolution and demonstrate that the relative differences between the mean reflectance at full resolution (4 km) and a degraded resolution (50% degradation) of 8 km is $\approx 3\%$. Uncertainties due to the spatial resolution problem would be smaller again for the present study as the initial pixel size difference (from Terra-MODIS to GMS-5/SVISSR) is only 25%. Intrinsic resolutions of Terra-MODIS (1 km) and GMS-5/SVISSR (1.25 km) observations being degraded before retrievals to a similar pixel size of 5 km, resolution effects will be significantly limited.

3.3.2. Spectral Channel Bandwidth

[16] A sensor is sensitive to incoming energy over a range of wavelengths. Each of these wavelengths contributes to the signal recorded. GMS-5/SVISSR visible channel bandwidth is wider than that of Terra-MODIS. Though the direct impact of this GMS-5/SVISSR bandwidth on COD retrievals cannot be firmly established, reflectances are obtained by integration of the sensor response function over the bandwidth. Additionally, the calibration procedure (as will be seen in section 3.4) should compensate for possible negative effects related to the GMS-5/SVISSR visible channel bandwidth.

3.3.3. Data Quantization

[17] As seen in section 2, Terra-MODIS data quantization is 12 bit while that of GMS-5/SVISSR is 6 bit (visible channel) and 8 bit (IR channels). The maximum uncertainty due to GMS-5/SVISSR channels’ low quantization is, for

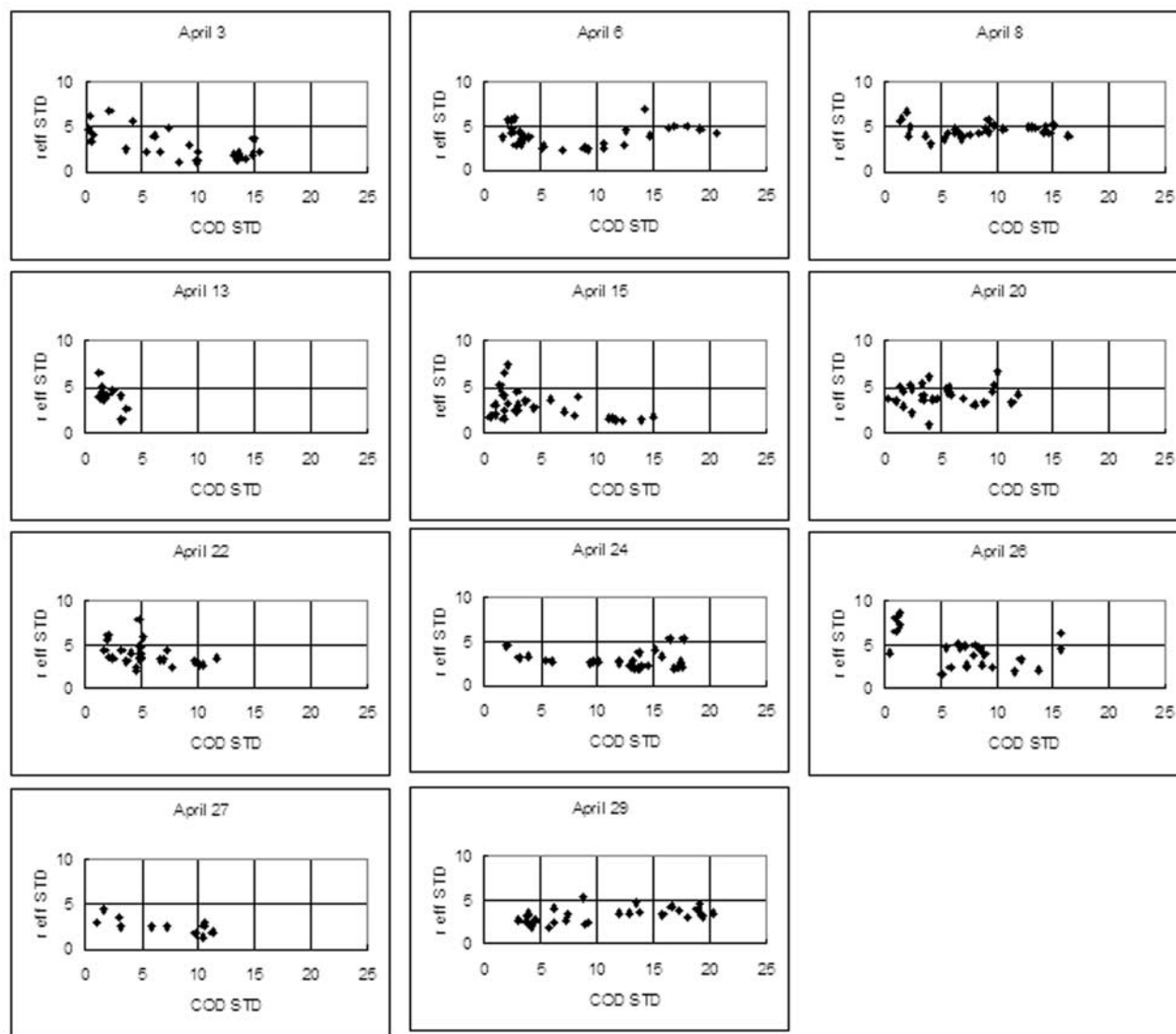


Figure 4. MODIS COD variability against cloud effective radius at brightness temperature intervals of 1 K. COD STD is MODIS' COD standard deviation; r eff STD is MODIS' cloud droplet effective radius standard deviation.

the brightness temperature ~ 0.57 K (evaluated at a BT of 220 K) and for the bidirectional reflectance, less than 0.016 (evaluated at an effective reflectance of ~ 1). The COD error related to this reflectance uncertainty is quite low (less than 1.5% at our maximum optical depth, i.e., 70).

3.4. Calibration and Geolocation Problems

[18] Since the launch of the GMS-5 satellite (1995), a gradual degradation of its sensors has been noticed. Because the visible channel of this satellite does not have onboard calibration, standard calibration techniques using ISCCP constants are applied on GMS-5/SVISSR reflected radiances, prior to COD retrievals in this study. These calibration constants are available on the ISCCP Web page and presented on a monthly basis in the form of a straight line equation including corrected and nominal scaled visible radiances.

[19] Regarding possible geolocation problems and in case there are, degrading the pixel initial size (case of our study:

All pixels were degraded to a size of 5×5 km²) may reduce to a negligible quantity their impact. To minimize the variance between the two satellites' data, as expressed by the RMSD, and obtain an optimum correlation of the spatial patterns, the shifting (collocation method) in various directions of the Terra-MODIS image relative to that of GMS-5/SVISSR was attempted. However, this did not much improve the quality of the data examined.

3.5. Cloud Inhomogeneity Effects

[20] The data selected from section 3.1 to section 3.4 can now be examined to understand the influence of cloud inhomogeneity on the satellites' retrievals. We'll try to know how the inhomogeneity of the cloud structure may affect the accuracy of the optical depth retrievals. The degree of cloud inhomogeneity and obliqueness of the viewing angles generally enhance 3-D radiative effects. These effects may be due to internal or external inhomogeneities. The internal cloud inhomogeneity radiative effects

are the result of the variation in the volume extinction coefficient and, consequently, the liquid (or ice) water content variation, while the external inhomogeneity effects refer to the relation between the cloud external structure and the solar illumination conditions. The external radiative effects are mainly the cloud asymmetry (reflectivity differences between illuminated and shadow cloud faces) and the structured cloud sides (differences in reflectivity, due to the slope of illumination). The internal inhomogeneity shows that areas with high water content generally correspond to high COD values. Though the water content property is generally highly correlated with COD, no trend showing the reduction or enhancement of COD values due to this factor was observed. As the cloud water content is well correlated with the cloud droplet effective radius, we will refer to section 3.2.2 for the examination of the impact of this factor. Regarding external inhomogeneity radiative effects, it was noticed on one hand that Terra-MODIS COD values are, on average, systematically larger than those of GMS-5/SVISSR at the shadow sides of the clouds, and statistically comparable values are observed as we move toward sunlit sides. On the other hand, the differences (positive and negative) are higher at steep (slope) cloud sides. The external inhomogeneity radiative effects will be quantitatively expressed in this study as simple COD differences, or RF and RD (relative difference), i.e., the ratio of COD difference between the two satellites to the Terra-MODIS COD, in %:

$$RD(\%) = \frac{MODIS_{COD} - SVISSR_{COD}}{MODIS_{COD}} \times 100 \quad (3)$$

4. Cloud Inhomogeneities Effects

4.1. Internal Inhomogeneities Effects

[21] Because satellite sensors can only view clouds at their surface, the effects of internal inhomogeneity tend to reflect clouds properties close to the cloud top surface. Cases of cloud multilayering and droplet size change with altitude, complex to handle with only satellite observations, are beyond the scope of our study. Cloud internal inhomogeneities result from the variation of the volume extinction coefficient, which is itself related to the cloud water content variation. The measure of the liquid (or ice) water content is generally expressed as the liquid water path (LWP in g/cm^2). The LWP is proportional to the cloud optical depth (τ_c) and the droplet effective radius (r_{eff} in μm). It is expressed by

$$LWP = 4/(3Q_{ext}) \tau_c r_{eff} \rho_w \quad (4)$$

where Q_{ext} is the average extinction efficiency over the droplet size distribution calculated from Mie scattering theory. Its value can be assumed equal to 2; ρ_w is the mass density of liquid water.

[22] The LWP is evaluated only with Terra-MODIS data, as the droplet effective radius cannot be retrieved with GMS-5/SVISSR data for the reasons stated in section 2. Results of this analysis show that the LWP is highly correlated to COD (correlation coefficient always above 0.85). The spatial variability of LWP evaluated through a 3×3 pixel standard deviation increases or decreases

proportionally to that of the COD. Such a result is generally expected for most homogeneous clouds. As the LWP is generally proportional to the cloud droplet effective radius, the study of the variability of this factor may be reduced to that of the cloud droplet effective radius. We will therefore mostly refer to section 3.2.2 for the analysis of the effect of internal inhomogeneity on the COD retrievals. The distribution of the cloud droplet effective radius as seen previously (Figure 3) shows that cold clouds are mostly composed of large particles effective radius generally above $15 \mu\text{m}$, while warm clouds' droplet radius is generally centered on $10 \mu\text{m}$. Cold clouds' COD estimated by Terra-MODIS are probably high because of their composition in mostly large particles. The water clouds' COD from the two satellites seem to be closer because of the high occurrence of droplet effective radius near $10 \mu\text{m}$ (value assumed for GMS-5/SVISSR). Furthermore, and as specified in the previous chapter (Figure 4), no specific correlation exists between the horizontal variation of water clouds' droplet effective radius at close altitudes and the equivalent horizontal COD variation. The impact of the effective radius on the water COD retrievals may be quite limited.

[23] Though the presence of inhomogeneities in the distribution of water within a cloud reduces the amount of absorption in this cloud [Cairns *et al.*, 2000], several studies suggest that 3-D radiative effects are more sensitive to the external inhomogeneity (asymmetry effect, structured cloud sides, or geometrical roughness, etc.) rather than internal inhomogeneity of the extinction coefficient [Loeb *et al.*, 1998; Varnai, 2000; Iwabuchi and Hayasaka, 2002]. Furthermore, a comparative study on effects of cloud inhomogeneity from Loeb *et al.* [1997] suggests that nadir reflectances show a much smaller sensitivity to internal than to external inhomogeneities.

4.2. External Inhomogeneities Effects

[24] The radiation received by satellite sensors is the result of interception and/or emission and multiple scattering of the photons hitting cloud surfaces. Clouds are inherently heterogeneous and require a three-dimensional viewpoint both in terms of their description and in order to understand their interaction with radiation [Varnai and Davies, 1999]. The effects of finite cloud geometry are analyzed with satellite observations mainly at infrared wavelengths. Cloud inhomogeneity studies often rely on such data. These reveal the shape of the surfaces controlling the direction and degree of reflection of solar radiation. Main cloud external inhomogeneity effects include cloud asymmetry, structured cloud side or roughness effects, preferential orientation, a mixture of small and large particles around the cloud surface (the presence of small particles in a cloud level is likely to raise the degree of scattering of solar radiation), etc. An evaluation of these properties reveals that the 3-D radiative effects having a quantifiable impact on the data examined in this study are the cloud asymmetry and structured cloud sides. Two methods are used for the detection of these effects. They rely on the determination of a local brightness temperature gradient around every pixel.

4.2.1. First Method

[25] This method is used to examine the radiative effect of asymmetry resulting from differences in the illumination

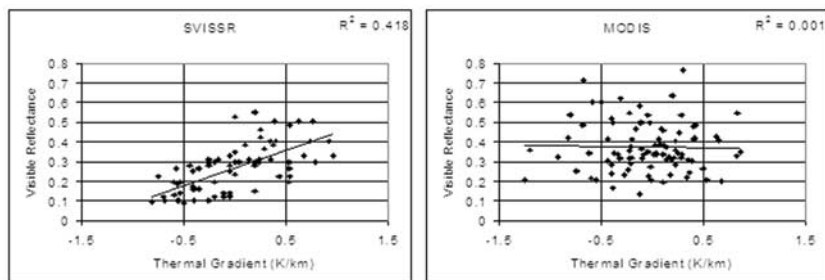


Figure 5. Reflectance versus local thermal gradient for pixels with brightness temperatures between 279 and 280 K on 6 April 2001.

of cloud surfaces, as well as that due to the degree of inclination of cloud sides (structured). To analyze these effects on the measured cloud properties, a simple technique of detection, as proposed by *Varnai and Marshak* [2002], is used. The method's basic idea is to estimate, for each basic pixel in the area, whether 3-D effects are likely to have increased or decreased the pixel's brightness at the visible channel relative to 1-D theory. The technique assumes that the question of whether 3-D effects enhance or reduce the brightness of a pixel depends mainly on whether the pixel is on a slope tilted toward (illuminated slopes) or away from the sun (shadowy slopes). The decision to classify a pixel as illuminated or shadowy is based on the direction of solar azimuth angle. For the scenes examined in this study the solar azimuth angle varies between 155 and 180° (from the north). A local gradient of the brightness temperature (g) is calculated from the pixels in front (T_{front} : brightness temperature in front) and behind (T_{behind} : brightness temperature behind) a central pixel facing the solar azimuth orientation:

$$g = (T_{\text{front}} - T_{\text{behind}})/d \quad (5)$$

with d = the distance separating the pixels in front and behind (10 km for this study). If $g > 0$, the pixel is on an illuminated slope; if $g < 0$, the pixel is on a shadowy slope.

[26] To understand these cloud radiative effects, analyses can be conducted at the macroscale or microscale levels. At the macroscale level, and as suggested by *Varnai and Marshak* [2002], an area of $50 \times 50 \text{ km}^2$ is chosen with the goal that it contains many pixels to allow statistical calculations but does not have clouds from different cloud fields too often. Then, after all cloudy pixels in the same area are designated as either illuminated or shadowy, the mean reflectance or COD of the illuminated and shadowy pixels is calculated. If the two mean values are close to each other, this indicates that 3-D effects do not make much of a difference in the $50 \times 50 \text{ km}^2$ area. If, however, it is much larger, 3-D effects are expected to be strong. Application of this technique to our study area shows that both GMS-5/SVISSR and Terra-MODIS data, in some cases, express slight brightness differences between illuminated and shadowy pixels. Radiative effects may not be clearly visible at this scale of study because of the areas' large pixel size. A better understanding of the phenomenon may be possible at the microscale level, i.e., a pixel-by-pixel study. Visible reflectance versus local brightness thermal gradient (as derived from (5)) within 1 K temperature difference is

examined for both satellites. Figure 5 is an illustration of this relationship, with the scene of 6 April chosen as a typical case. The graphs presented show the existence of a quantifiable relation ($R^2 = 0.4$) between these parameters for the case of GMS-5/SVISSR data, while MODIS data present a poor correlation. Reflectance values of GMS-5/SVISSR tend to increase with the degree of illumination as illustrated by the negative to positive brightness temperature gradient trend (i.e., from shadowy to illuminated pixels). Despite the relatively degraded pixel size used for this study, the impact of 3-D radiative effects due to cloud asymmetry is noticeable with the GMS-5/SVISSR reflectance data used. The dependence of GMS-5/SVISSR reflectance on the cloud surface brightness means that the illuminated surfaces are either too bright or the shadow surfaces are too dark. To understand the incidence of the relation of GMS-5/SVISSR visible reflectance–cloud surface thermal gradient (i.e., the impact of the illumination conditions on cloud faces) on COD retrievals, and consequently the discrepancies between the two satellites, we can compare the average COD obtained from the illuminated and shadowy groups of pixels. The comparison made shows (Figure 6) that GMS-5/SVISSR illuminated pixels' COD are always higher on average than those of the shadow sides. This is not often the case for Terra-MODIS data. As a consequence, the RF and the COD difference (MODIS – SVISSR) are systematically higher at the shadow sides of the clouds. At the illuminated cloud sides the discrepancies are substantially reduced (both the RF and the COD difference substantially decrease), and GMS-5/SVISSR pixels mostly show higher values than those of Terra-MODIS. The correlation between brightness temperature gradient and reflectance, well noticed with GMS-5/SVISSR data and poorly remarkable with MODIS data, and the differences in the COD retrievals suggest that GMS-5/SVISSR COD are underestimated at shadow cloud faces and overestimated at illuminated sides. As illustrated also by Figure 6, the relative difference between the COD from the illuminated cloud sides and those from the shadow sides can be as high as 30% or exceed this value. For a given parameter the degree of dispersion of the differences between two data sets may be easily expressed by the RMSD. Regarding our study, the dispersion noticed in the COD data as revealed by the RMSD (Figure 6) could be due either to time or navigation differences between GMS-5/SVISSR and Terra-MODIS satellites. Small time differences in the images of only a few minutes are sufficient to introduce significant variations for regions less than 50 km wide

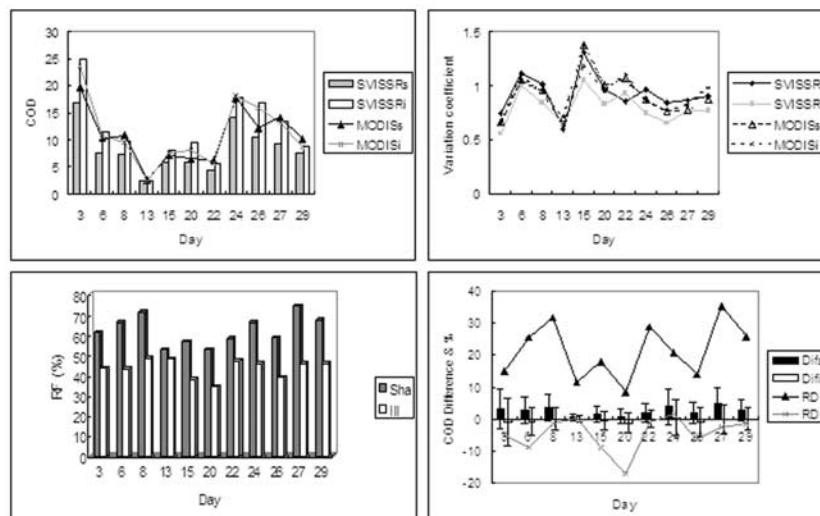


Figure 6. Average COD (top, left) and corresponding variation coefficient (top, right), RF (bottom, left), and COD differences (MODIS – SVISSR) (bottom, right) for all the days analyzed. Indices “s” and “i” represent shadowy and illuminated pixels, respectively. Difs and Difi are COD differences (MODIS – SVISSR) at shadow and illuminated sides, respectively. Vertical bars (bottom, right) are the COD RMSD between GMS-5/SVISSR and Terra-MODIS.

[Minnis *et al.*, 1993]. Other dispersion parameters for the COD could be the cloud droplet effective radius variations, etc.

[27] The other 3-D radiative effect examined in this study is that of the structured cloud sides. In order to understand the magnitude of the variation of this effect or how much the COD retrievals deviate from a plane-parallel homogeneous surface (as commonly assumed in the radiative transfer model calculations), the following interpretations of brightness temperature (thermal gradient) data are conducted. This means we examine how the slope of the cloud surface influences optical depth differences between GMS-5/SVISSR and Terra-MODIS. For this purpose, local brightness temperature gradients are sorted in bins of 0.5 K/km. Figure 7 shows the results obtained and expressed as a function of RD (%) for all the matching scenes (except 13 and 27 April where the gradients are generally low and essentially comprised in the range ± 0.5 K/km), i.e., the variation of RD (%) with the brightness temperature gradient. The results obtained show that the lowest COD discrepancies (RD in absolute value is near 0) occur at the lowest gradient range (± 0.5 K/km), or near-plane-parallel surfaces. Most of these gradients are on the illuminated cloud sides. The slope of the shadow faces increases with RD; that is, Terra-MODIS values are gradually higher than those of GMS-5/SVISSR, while at the illuminated sides both satellites’ COD show closer values. Additionally, at the highest slopes of the latter sides, GMS-5/SVISSR values tend to be higher than those of Terra-MODIS. Three-dimensional radiative effects therefore increase with the slope of the cloud surface. Similarly, the COD difference between the two satellites increases with the slope; that is, at shadow sides of the clouds GMS-5/SVISSR COD are generally lower, while at illuminated sides, they are greater. The results shown above, i.e., the local brightness temperature gradients, indicate that COD data within gradients of ± 0.5 K/km, i.e., near-plane-parallel surfaces, are the most

reliable (as they present the lowest RD). Without a prior knowledge of the cloud surface structures, and due to the rigidity of most common retrieval models, 3-D radiative effects are generally not taken into account during COD retrievals by plane-parallel radiative transfer models. Cloud top surface, for example, of a surrounding anvil may bias the retrieved optical depth from visible radiances if the incoming sunlight is obscured by a convective overshoot [van Hees and Lelieveld, 2000].

[28] So far the relationship between the COD difference and the degree of illumination has been examined for the whole range of water cloud temperatures. To verify if this relationship is not temperature dependent, average COD data of the illuminated and shadow pixels corresponding to consecutive temperature intervals of 5 K are compared. The plots obtained and presented in Figure 8 show that the GMS-5/SVISSR average COD values at illuminated cloud sides are significantly higher than that at shadow cloud sides and this, indistinctly at lower, intermediate, or higher temperatures intervals (Figure 8, left to right). A slightly similar trend is noticed with Terra-MODIS data but the differences between the illuminated and shadow sides’ COD are very narrow. The comparison between both satellites’ data shows that, at any temperature, GMS-5/SVISSR average COD is always higher than that of Terra-MODIS at the illuminated cloud sides, while it is the opposite at the shadow cloud sides. The trend of the COD variation in each satellite, or the COD difference between both satellites, with the degree of illumination, does not show any preferential temperature dependence. There is therefore no temperature bias of the 3-D radiative effects.

4.2.2. Second Method: Edge Enhancement

[29] More refined than the previous method, the edge enhancement method provides the possibility to examine the effects of asymmetry and structured cloud sides at various directions. This method takes advantage of particular properties offered by the use of edge enhancement

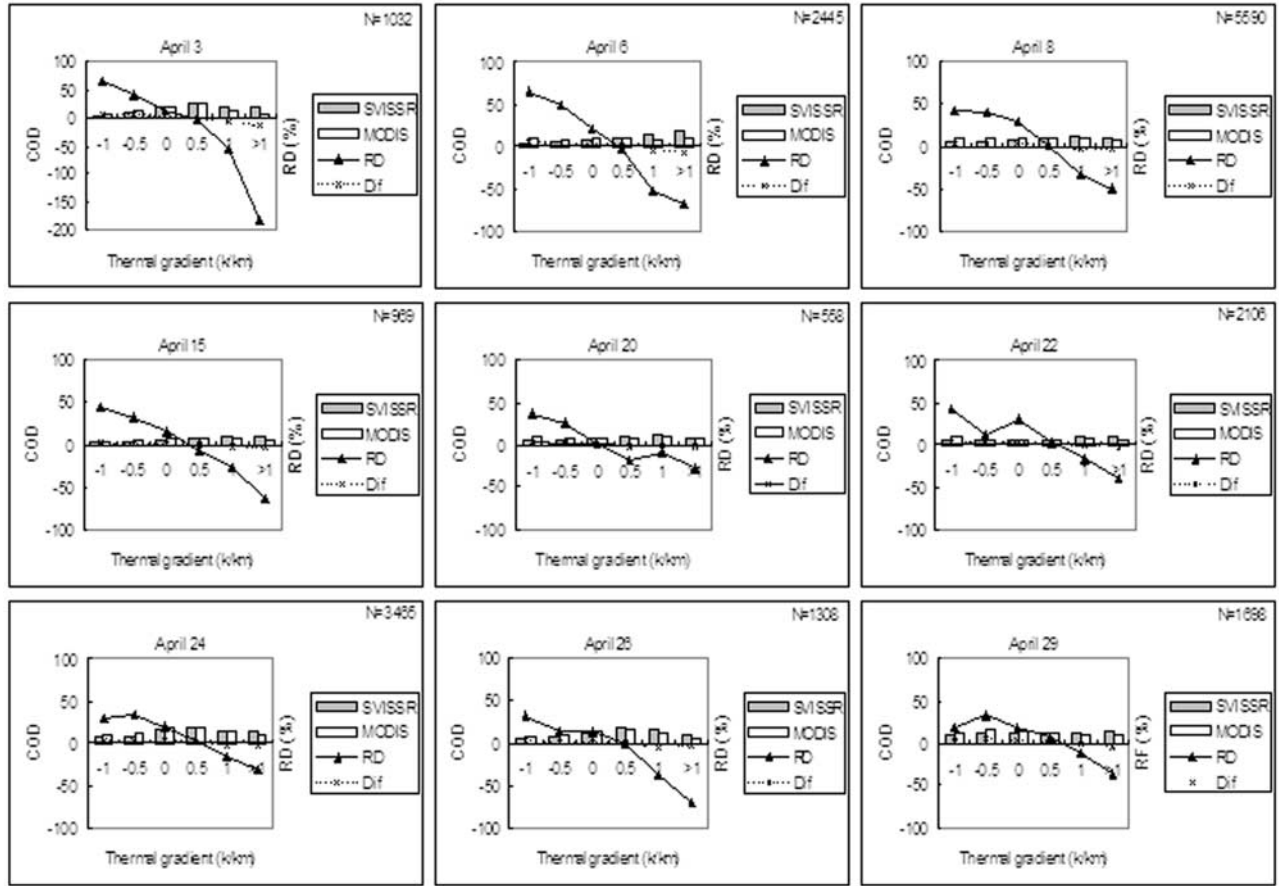


Figure 7. Thermal gradient distributions as a function of COD and relative difference (RD). N represents the total number of data.

operators. Such operators can be employed to enhance the brightness contrast at the edges between illuminated and shadow pixels of an image. They can be efficient in locating sharp changes in the intensity function of radiation, allowing therefore the study of a particular property of the brightened surface. The theoretical background of this method as applied in our study is described by *van Hees and Lelieveld* [2000]. Using the Sobel edge enhancement operator, a local gradient around a central point, $A(i, j)$,

$$\begin{vmatrix} A_0 & A_1 & A_2 \\ A_3 & A(i, j) & A_5 \\ A_6 & A_7 & A_8 \end{vmatrix} \quad (6)$$

representing a 3×3 pixel, can be determined. Estimates of the gradient derivatives in the x and y directions are, respectively,

$$G_x = (A_2 + 2A_5 + A_8) - (A_0 + 2A_3 + A_6) \quad (7)$$

$$G_y = (A_0 + 2A_1 + A_2) - (A_6 + 2A_7 + A_8) \quad (8)$$

The gradient operator is defined finally as

$$G(i, j) = \sqrt{G_x^2 + G_y^2} \quad (9)$$

The direction of this gradient is given by

$$\phi_G = \arctan\left(\frac{G_y}{G_x}\right) \quad (10)$$

[30] For the sake of simplicity, data from all the thermal gradient directions (on a complete circle) can be grouped in four intervals. According to the solar azimuth angle of the scenes selected, cloud faces will be designated as shadow side ($\phi_G \geq 45^\circ$ and $\phi_G \leq 135^\circ$), left side ($\phi_G > -45^\circ$ and $\phi_G < 45^\circ$), right side ($\phi_G < -135^\circ$ and $\phi_G \geq 135^\circ$), and illuminated side ($\phi_G \geq -135^\circ$ and $\phi_G \leq -45^\circ$).

[31] To examine the possible influence of the illumination contrast between cloud sides on the data retrieved from the two satellites, the Sobel gradient operator and direction of the illuminated pixels (assigned a positive sign) and shadow pixels (assigned a negative sign) are plotted against the corresponding reflectance for close IR BT (i.e., within 1 K difference). As in section 4.2.1, the scene of 6 April is chosen to illustrate this relationship (Figure 9). *GMS-5/SVISSR* reflectance tends to increase with the Sobel gradient, while only a poor correlation is noticed with *Terra-MODIS* data. The effects of these relationships on COD retrievals and differences between the two satellites can be quantified. As shown in Figure 10, the highest COD differences (i.e., when *GMS-5/SVISSR* COD are lower than those of *Terra-MODIS*) are noticed in the shadow group of pixels.

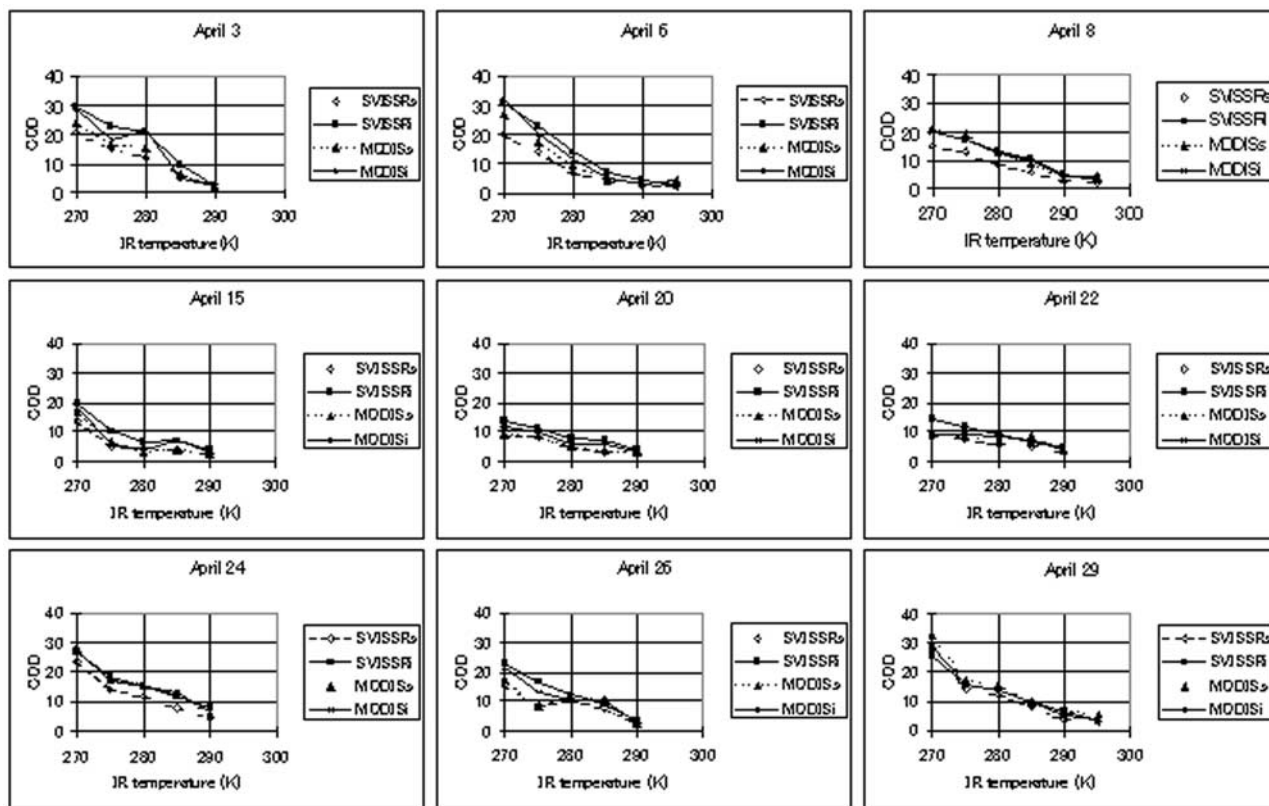


Figure 8. Average COD corresponding to BT intervals of 5 K for shadow and illuminated cloud sides' conditions. Indices "s" and "i" represent shadowy and illuminated pixels, respectively.

Left and right cloud sides show reduced differences, with, however, Terra-MODIS data still slightly higher. On the illuminated pixels the GMS-5/SVISSR COD are on average similar or higher than that of Terra-MODIS. These results expressed in terms of COD differences (the RF variation having a similar trend) between the two satellites confirm the trend noticed with the first method of analysis of the 3-D radiative effects, but also allow for a better distinction of the cloud illumination patterns. The difference between illuminated and shadowy pixels of Terra-MODIS is on average smaller than that of GMS-5/SVISSR as can be seen on the middle and right histograms of Figure 10.

4.2.3. Discussion of the External Inhomogeneities Effects

[32] In this study, both the unidirectional method (first method) and the edge enhancement method (second method)

were used to examine how and at which extent cloud horizontal inhomogeneity observed from satellite data can influence optical property retrievals. As previously stated, the plane-parallel homogeneous assumption in radiative transfer models uses horizontally averaged optical properties to calculate the cloud optical depth. The transport of photons along cloud faces or the average COD obtained depends on the balance between illuminated and shadowy components of the cloud. The higher COD observed on illuminated cloud faces compared to that of the shadowy ones is due to the stronger upward escape of solar rays from the former cloud surfaces. Because of the shorter path of the three-dimensionally reflected photon compared to that of the one-dimensional homogeneous reflection, the COD are likely to be higher at high slopes of the illuminated faces than at horizontal cloud surfaces. Regarding the spatial

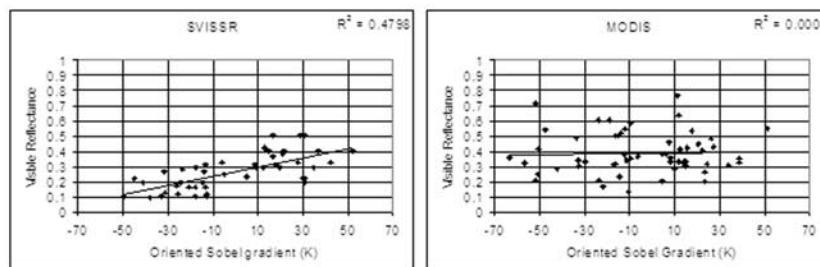


Figure 9. Visible reflectance versus oriented Sobel gradient for shadowy and illuminated pixels with brightness temperatures between 279 and 280 K on 6 April 2001. Positive gradient values are pixels on the illuminated cloud sides, and negative gradient values are pixels on the shadow cloud sides.

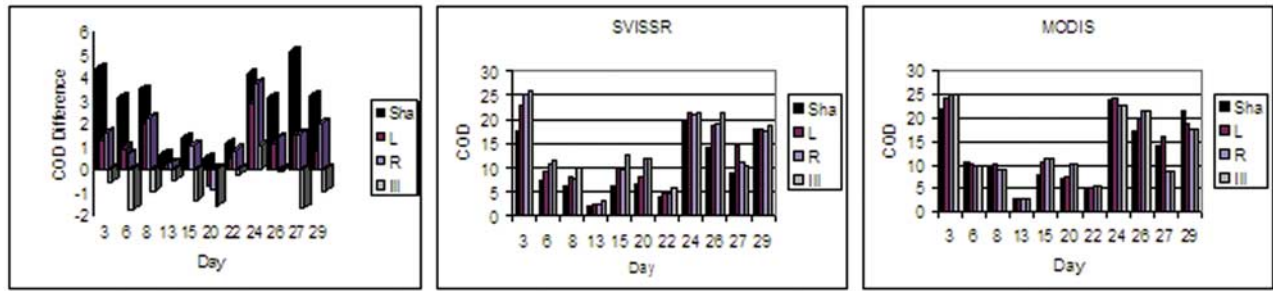


Figure 10. Mean COD difference (left), GMS-5/SVISSR COD (middle), and Terra-MODIS COD (right), according to the illumination conditions for an entire cloud scene. (Sha = shadowy side pixels, L = left side of the illuminated pixels, R = right side of the illuminated pixels, and Ill = illuminated pixels).

resolution, we intuitively expect the apparent variability of cloud fields to be smaller when they are observed with coarse-resolution sensors or when high-resolution measurements are degraded to lower resolution [Oreopoulos and Davies, 1998]. Radiative effects are enhanced when this variability is higher. As an illustration, Figure 11 shows the

degree of variation or dispersion of water cloud reflectance (variation coefficient: ratio of standard deviation to average) versus the brightness temperature. In most of the scenes the variability of GMS-5/SVISSR reflectance is higher than that of Terra-MODIS. This would explain why 3-D radiative effects are mostly observed in GMS-5/SVISSR data.

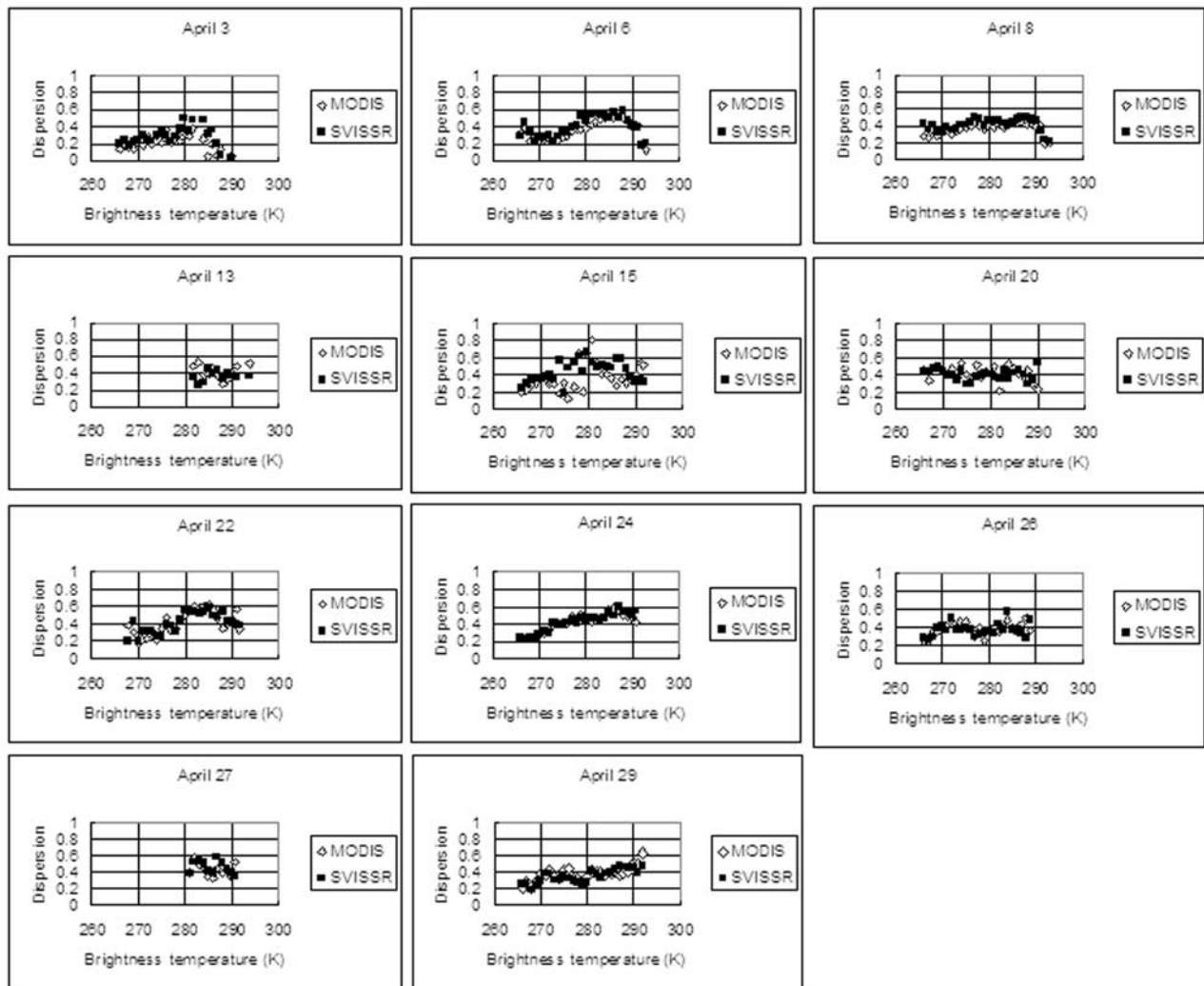


Figure 11. Cloud reflectance variability expressed by the reflectance dispersion coefficient (ratio of standard deviation to average) versus brightness temperature.

Though the GMS-5/SVISSR COD differences between the illuminated and shadow pixels may be sometimes relatively high, there is some compensation effect between clouds' COD quantities when averages are calculated. Consequently, the COD differences between GMS-5/SVISSR and Terra-MODIS may not be very large.

[33] Another evaluation of the variability of the daily COD as also expressed by the COD variation coefficient (ratio of COD standard deviation to average) of illuminated and shadowy cloud pixels separately and plotted in Figure 6 (top, right), shows that GMS-5/SVISSR shadowy cloud pixels may be less reliable than illuminated cloud pixels (higher variability of shadow cloud sides than that of illuminated cloud sides), and no real difference exists between illuminated and shadowy cloud pixels of Terra-MODIS (similar variability of both sides of cloud pixels). Equivalent plots done with reflectance data show similar trends as those with the COD.

[34] Some distortions in cloud shape images by GMS-5/SVISSR have been noticed over Southeast Asia [Kitamoto and Ono, 2001], a location having satellite-viewing angles almost similar to those of our study area. These distortions have negative effects over shadowy cloud pixels and positive effects over illuminated cloud pixels (the data examined in our study show that negative effects are stronger than positive effects). They may therefore be suspected as one of the factors explaining the higher prevalence of 3-D radiative effects with GMS-5/SVISSR data than with those of Terra-MODIS. The enhancement of reflectance at illuminated clouds and its reduction at shadow clouds of GMS-5/SVISSR result, respectively, in higher and lower 1-D optical depth retrievals. Another suspected factor could be the broad bandwidth of GMS-5/SVISSR compared to the narrow bandwidth of Terra-MODIS. Instinctively, the broader the range of wavelengths, the more energy there is available to be recorded. A broad bandwidth therefore is expected to produce a strong signal (as probably reflected by GMS-5/SVISSR illuminated cloud sides), though decreasing the spectral resolution.

5. Conclusions

[35] Because clouds are dynamic features, they need to be monitored at short time intervals in order to accurately assess their contribution in the distribution of global radiation. A good and efficient tool to do this is to use geostationary satellites. However, before using data derived from such satellites, the degree of accuracy of the retrieved products needs to be validated. The validation scheme often used is the comparison of these data with ground-truth observations or with a higher spatial resolution low-altitude satellite. The present study used the latter approach to assess the quality of cloud microphysical and optical properties derived from GMS-5/SVISSR over a region off the southeast China Sea. GMS-5/SVISSR derived COD data were compared with those of the polar orbiting satellite Terra-MODIS. This comparison showed discrepancies between both sets of data. GMS-5/SVISSR COD appeared in most of the scenes, lower than those of Terra-MODIS. The reasons for these differences were investigated. Factors likely to influence satellite cloud observations and retrievals were then discussed, with a particular stress on the role of cloud

inhomogeneities. These reasons were in order: satellite viewing and solar geometries, cloud phase differentiation and cloud particle effective radius, sensors' resolution, spectral channel bandwidth and data quantization, calibration and geolocation problems, and cloud inhomogeneities induced 3-D radiative effects. The data noticeably affected by any of the first four factors were progressively discarded. The restrictive data sets resulting from this selection were then analyzed in order to understand the impact of the last factor, i.e., the cloud inhomogeneity effects on COD retrievals. To avoid biases due to observation conditions' differences between both satellites, similar viewing geometries data only were selected in the initial step of analyses. The COD data obtained showed persistent differences. The cloud phase analysis following this step showed that the frequency of Terra-MODIS pixels with a higher COD than that of GMS-5/SVISSR was regularly larger in ice clouds than in water clouds. The COD discrepancies between the satellites used were mostly seen with Cb clouds (cold clouds). The same behavior was noticed for cold Ci clouds. The Cu clouds (warm clouds), as well as warm Ci, showed comparable values. The large differences (MODIS – SVISSR) in the ice cloud values may suggest that ice phase interpretation with a water droplet algorithm could be problematic, the distribution of the cloud particle effective radius as well. The choice of a water cloud particle radiative transfer model to analyze a 2-phase cloud radiation data may produce large uncertainties in ice cloud optical depth retrievals of at least one of the satellites. Comparison of water cloud data between both satellites showed that though the COD differences still existed, they were significantly reduced. Furthermore, the distribution of the cloud droplet effective radius showed that cold clouds were mostly composed of large particles' radius generally above 15 μm , while warm clouds droplet radius was generally centered on 10 μm . Cold clouds COD estimated by Terra-MODIS were probably high because of the fact that they are mostly composed by large particles. The water clouds COD from the two satellites seem to be closer because of the high occurrence of droplets effective radius near 10 μm (value assumed for GMS-5/SVISSR).

[36] For the rest of the analyses of this study, only water cloud data were used. Among the other factors influencing the COD retrievals, emphasis was put on inhomogeneities induced 3-D radiative effects. These effects were mainly the cloud asymmetry and structured cloud sides. To analyze them, two approaches were adopted. These are based on the use of a local brightness temperature gradient and its orientation. The examination of the radiative effects on a pixel-by-pixel basis revealed the existence of a quantifiable correlation between GMS-5/SVISSR cloud reflectance and BT gradient. Cloud reflectance clearly increased with the degree of illumination, i.e., from shadow to illuminated sides. A poorer correlation was detected with Terra-MODIS data. The consequence of the correlation noticed with GMS-5/SVISSR data was that the relative frequency of Terra-MODIS pixels with COD values higher than those of GMS-5/SVISSR was always larger in the shadowy group of pixels, then decreased or became smaller in the illuminated group. GMS-5/SVISSR average COD at illuminated cloud sides were largely higher than that at shadow cloud sides. An ambivalent trend was noticed with Terra-MODIS

data as COD differences between the illuminated and shadow sides appeared quite narrow. Differences of COD between both satellites (MODIS – SVISSR) were systematically higher at the shadow sides of the clouds and substantially reduced toward the illuminated cloud sides. GMS-5/SVISSR pixels were even higher than those of MODIS at high gradients of the illuminated pixels. Furthermore, it was noticed that the lowest COD discrepancies occurred at low thermal gradients and more specifically at the slightly inclined illuminated faces, which are indeed the closest to a plane-parallel surface. These facts suggest that GMS-5/SVISSR pixels might be too dark at the shadow sides of the clouds and too bright at the illuminated sides. The good and poor correlation between cloud reflectance and the corresponding brightness temperature gradient with GMS-5/SVISSR and Terra-MODIS data, respectively, might suggest that GMS-5/SVISSR COD retrievals were underestimated at shadow cloud sides and overestimated at illuminated sides. The results shown in section 4.2.1 indicate that COD data within ± 0.5 K/km gradients, i.e., near-plane-parallel surfaces, were the most reliable as they have the lowest COD relative difference. The COD difference between both satellites increased with the cloud side slope. At any temperature of the illuminated cloud sides, GMS-5/SVISSR average COD was always higher than that of Terra-MODIS, while it was the opposite for the shadow cloud sides. The water cloud COD difference between both satellites did not show any preferential temperature dependence; that is, there was no temperature-illumination bias in the COD data. As satellite retrievals are based on a 1-D theory, 3-D radiative transfer effects are not generally taken into account prior to cloud optical properties retrievals.

[37] The cloud inhomogeneity-related influences examined in this study for water clouds are expected to be more significant for ice clouds because most of these clouds have a strong vertical development. This development automatically generates steep slopes at cloud sides. The latter strongly enhance the cloud inhomogeneity radiative effects, making therefore illuminated and shadow clouds much brighter and darker, respectively.

[38] **Acknowledgments.** This research was materially supported by the Japan Society for the Promotion of Science (JSPS). We would like to thank them here for making this study possible.

References

- Brest, C. L., W. B. Rossow, and M. D. Roiter (1997), Update of radiance calibrations for ISCCP, *J. Atmos. Oceanic Technol.*, *14*, 1091–1109.
- Cahalan, R. F., W. Ridgway, W. J. Wiscombe, T. L. Bell, and J. B. Snider (1994), The albedo of fractal stratocumulus clouds, *J. Atmos. Sci.*, *51*, 2434–2455.
- Cairns, B., A. A. Lacis, and B. E. Carlson (2000), Absorption within inhomogeneous clouds and its parameterization in general circulation models, *J. Atmos. Sci.*, *57*, 700–714.
- Casanova, C., A. Romo, E. Hernandez, J. L. Casanova, and J. Sanz (2005), Rapid response for cloud monitoring through Meteosat VIS-IR and NOAA-A/TOVS image fusion: Civil aviation application. A first approach to MSG-SEVIRI, *Int. J. Remote Sens.*, *26*(8), 1699–1716.
- Chang, F., Z. Li, and S. A. Ackerman (2000), Examining the relationship between cloud and radiation quantities derived from satellite observations and model calculations, *J. Clim.*, *13*, 3842–3859.
- Desormeaux, Y., W. B. Rossow, C. L. Brest, and G. G. Campbell (1993), Normalization and calibration of geostationary satellite radiances for the International Satellite Cloud Climatology project, *J. Atmos. Oceanic Technol.*, *10*, 304–325.
- Houghton, J. (2002), *The Physics of Atmospheres*, 3rd ed., Cambridge Univ. Press, New York.
- Inoue, T. (1987), A cloud type classification with NOAA 7 split-window measurements, *J. Geophys. Res.*, *92*, 3991–4000.
- Iwabuchi, H., and T. Hayasaka (2002), Effects of cloud horizontal inhomogeneity on the optical thickness retrieved from moderate resolution satellite data, *J. Atmos. Sci.*, *59*, 2227–2242.
- Kawamoto, K., T. Nakajima, and T. Y. Nakajima (2001), A global determination of cloud microphysics with AVHRR remote sensing, *J. Clim.*, *14*, 2054–2068.
- Kitamoto, A., and K. Ono (2001), The collection of typhoon image data and the establishment of typhoon information databases under international research collaboration between Japan and Thailand, *Natl. Inst. Inform. J.*, *2*(3), 15–26.
- Kriebel, K. T., G. Gesell, M. Kästner, and H. Mannstein (2003), The cloud analysis tool APOLLO: Improvements and validation, *Int. J. Remote Sens.*, *24*, 2389–2408.
- Le Marshall, J. F., J. J. Simpson, and J. Zonghai (1999), Satellite calibration using collocated nadir observation technique: Theoretical basis and application to the GMS-5 pathfinder benchmark period, *IEEE Trans. Geosci. Remote Sens.*, *37*(1), 499–507.
- Loeb, N. G., and J. A. Coakley Jr. (1998), Inference of marine stratus cloud optical depths from satellite measurements: Does 1D theory apply?, *J. Clim.*, *11*, 215–232.
- Loeb, N. G., T. Varnai, and R. Davies (1997), Effect of cloud inhomogeneities on the solar zenith angle dependence of nadir reflectance, *J. Geophys. Res.*, *102*, 9387–9396.
- Loeb, N. G., T. Varnai, and D. M. Winker (1998), Influence of subpixels-scale cloud-top structure on reflectances from overcast stratiform cloud layers, *J. Atmos. Sci.*, *55*, 2960–2973.
- Marshak, A., A. Davis, R. F. Cahalan, and W. Wiscombe (1998), Nonlocal independent pixel approximation: Direct and inverse problems, *IEEE Trans. Geosci. Remote Sens.*, *36*, 192–205.
- Meteorological Satellite Center (MSC) (1997), *The GMS User's Guide*, 3rd ed., 190 pp., Meteorol. Satell. Cent. of Jpn., Jpn. Meteorol. Agency, Tokyo.
- Minnis, P., P. W. Heck, and D. F. Young (1993), Inference of cirrus cloud properties using satellite-observed visible and infrared radiances. part II: Verification of the theoretical cirrus radiative properties, *J. Atmos. Sci.*, *50*(9), 1305–1322.
- Minnis, P., L. Nguyen, D. R. Doelling, D. F. Young, W. F. Miller, and D. P. Kratz (2002), Rapid calibration of operational and research meteorological satellite imagers. part I: Evaluation of research satellite visible channels as references, *J. Atmos. Oceanic Technol.*, *19*(9), 1233–1249.
- Nakajima, T., and T. Nakajima (1995), Wide-area determination of cloud microphysical properties from NOAA AVHRR measurements for FIRE and ASTEX regions, *J. Atmos. Sci.*, *52*, 4043–4059.
- Nakajima, T., and M. Tanaka (1988), Algorithms for radiative intensity calculations in moderately thick atmospheres using truncation approximation, *J. Quant. Spectrosc. Radiat. Transfer*, *40*, 51–69.
- Nakajima, T., et al. (2003), Significance of direct and indirect radiative forcings of aerosols in the East China Sea region, *J. Geophys. Res.*, *108*(D23), 8658, doi:10.1029/2002JD003261.
- Nowicki, G. D., M. L. Nordeen, P. W. Heck, D. R. Doelling, M. M. Khaiyer, P. Minnis, and S. Sun-Mack (2003), Cloud microphysical and radiative properties derived from MODIS, VIRS, AVHRR, and GMS data over the tropical western Pacific, paper presented at the 13th Atmospheric Radiation Measurement (ARM) Science Team Meeting, U.S. Dep. of Energy, Broomfield, Colo., 31 March to 4 April. (Available at http://www-pm.larc.nasa.gov/arm_refs.html)
- Oreopoulos, L., and R. Davies (1998), Plane-parallel albedo biases from satellite observations. part I: Dependence on resolution and other factors, *J. Clim.*, *11*, 919–932.
- Picon, L., and M. Desbois (1995), High level moisture observations and derived parameters from Meteosat and other geostationary satellites, *Adv. Space Res.*, *16*(10), 73–86.
- Rossow, W. B. (1989), Measuring cloud properties from space: A review, *J. Clim.*, *2*, 201–213.
- Rossow, W. B., and L. C. Garder (1993), Cloud detection using satellite measurements of infrared and visible radiances for ISCCP, *J. Clim.*, *6*, 2341–2369.
- Rossow, W. B., Y. Desormeaux, C. L. Brest, and A. Walker (1992), International Satellite Cloud Climatology Project (ISCCP) radiance calibration report, *WMO/TD 520*, World Clim. Res. Programme, Geneva, Switzerland.
- van Hees, R. M., and J. Lelieveld (2000), Retrieving cloud top structure from infrared satellite data, *J. Geophys. Res.*, *105*(D12), 15,663–15,672.
- Varnai, T. (2000), Influence of three-dimensional radiative effects on the spatial distribution of shortwave cloud reflection, *J. Atmos. Sci.*, *57*, 216–229.

- Varnai, T., and R. Davies (1999), Effects of cloud heterogeneities on short-wave radiation: comparison of cloud-top variability and internal heterogeneity, *J. Atmos. Sci.*, *56*, 4206–4224.
- Varnai, T., and A. Marshak (2001), Statistical analysis of the uncertainties in cloud optical depth retrievals caused by three-dimensional radiative effects, *J. Atmos. Sci.*, *58*, 1540–1548.
- Varnai, T., and A. Marshak (2002), Observations of three-dimensional radiative effects that influence MODIS cloud optical thickness retrievals, *J. Atmos. Sci.*, *59*, 1607–1618.
- Yi, H. Y., P. Minnis, L. Nguyen, and D. R. Doelling (2001), A proposed multiangle satellite data set using GEO, LEO and Triana, paper presented at the 11th AMS Conference on Satellite Meteorology and Oceanography, Am. Meteorol. Soc., Madison, Wisconsin, 12–16 Oct. (Available at <http://www-pm.larc.nasa.gov/triana.html>)
-
- J. R. Dim, I. Okada, and T. Takamura, Center for Environmental Remote Sensing, Chiba University, 1-33 Yayoi-cho, Inage-ku, Chiba 263-8522, Japan. (dim@ceres.cr.chiba-u.ac.jp; iokada@ceres.cr.chiba-u.ac.jp; takamura@ceres.cr.chiba-u.ac.jp)
- T. Y. Nakajima, Department of Network and Computer Engineering, School of Engineering II, Tokai University, 2-28-4, Tomigaya, Shibuya-ku, Tokyo 151-0063, Japan. (nkjm@yoyogi.ycc.u-tokai.ac.jp)
- H. Takenaka, Graduate School of Science and Technology, Chiba University, 1-33 Yayoi-cho, Inage-ku, Chiba 263-8522, Japan. (takenaka_ceres@graduate.chiba-u.jp)